Three-Body Forces and the Limit of Oxygen Isotopes

Takaharu Otsuka,[1,2,3] Toshio Suzuki,[4] Jason D. Holt,[5] Achim Schwenk,[5] and Yoshinori Akaishi[6]

[1]*Department of Physics, University of Tokyo, Hongo, Tokyo 113-0033, Japan*
[2]*Center for Nuclear Study, University of Tokyo, Hongo, Tokyo 113-0033, Japan*
[3]*National Superconducting Cyclotron Laboratory, Michigan State University, East Lansing, Michigan, 48824, USA*
[4]*Department of Physics, College of Humanities and Sciences, Nihon University, Sakurajosui 3, Tokyo 156-8550, Japan*
[5]*TRIUMF, 4004 Wesbrook Mall, Vancouver, BC, V6T 2A3, Canada*
[6]*RIKEN Nishina Center, Hirosawa, Wako-shi, Saitama 351-0198, Japan*

(Received 17 August 2009; published 13 July 2010)

The limit of neutron-rich nuclei, the neutron drip line, evolves regularly from light to medium-mass nuclei except for a striking anomaly in the oxygen isotopes. This anomaly is not reproduced in shell-model calculations derived from microscopic two-nucleon forces. Here, we present the first microscopic explanation of the oxygen anomaly based on three-nucleon forces that have been established in few-body systems. This leads to repulsive contributions to the interactions among excess neutrons that change the location of the neutron drip line from ^{28}O to the experimentally observed ^{24}O. Since the mechanism is robust and general, our findings impact the prediction of the most neutron-rich nuclei and the synthesis of heavy elements in neutron-rich environments.

DOI: 10.1103/PhysRevLett.105.032501 PACS numbers: 21.10.−k, 21.30.−x, 21.60.Cs, 27.30.+t

One of the central challenges of nuclear physics is to develop a unified description of all nuclei created in the laboratory and the cosmos based on the underlying forces between neutrons and protons (nucleons). This involves understanding the sequences of isotopes in the nuclear chart, Fig. 1, from the limits of proton-rich nuclei to the neutron drip line. These limits have been established experimentally up to oxygen with proton number $Z = 8$. Mapping out the neutron drip line for larger Z [1] and exploring unexpected structures in neutron-rich nuclei are a current frontier in the physics of rare isotopes. The years of discovery in Fig. 1 highlight the tremendous advances made over the last decade.

Figure 1 shows that the neutron drip line evolves regularly with increasing proton number, with an odd-even bound-unbound pattern due to neutron halos and pairing effects. The only known anomalous behavior is present in the oxygen isotopes, where the drip line is strikingly close to the stability line [2]. Already in the fluorine isotopes, with one more proton, the drip line is back to the regular trend [3]. In this Letter, we discuss this puzzle and show that three-body forces are necessary to explain why ^{24}O [4,5] is the heaviest oxygen isotope.

Three-nucleon ($3N$) forces were introduced in the pioneering work of Fujita and Miyazawa (FM) [6] and arise because nucleons are composite particles. The FM $3N$ mechanism is due to one nucleon virtually exciting a second nucleon to the $\Delta(1232$ MeV) resonance, which is deexcited by scattering off a third nucleon, see Fig. 3(e).

Three-nucleon interactions arise naturally in chiral effective field theory (EFT) [7], which provides a systematic basis for nuclear forces, where nucleons interact via pion exchanges and shorter-range contact interactions. The resulting nuclear forces are organized in a systematic expansion from leading to successively higher orders, and include the Δ excitation as the dominant part of the leading $3N$ forces [7]. The quantitative role of $3N$ interactions has been highlighted in recent *ab initio* calculations of light nuclei with $A = N + Z \leq 12$ [8,9].

We first discuss why the oxygen anomaly is not reproduced in shell-model calculations derived from microscopic NN forces. This can be understood starting from the stable ^{16}O and adding neutrons into single-particle orbitals (with standard quantum numbers nlj) above the ^{16}O core. We will show that correlations do not change this intuitive picture. Starting from ^{16}O, neutrons first fill the $0d_{5/2}$ orbitals, with a closed subshell configuration at ^{22}O ($N = 14$), then the $1s_{1/2}$ orbitals at ^{24}O ($N = 16$), and finally the $0d_{3/2}$ orbitals at ^{28}O ($N = 20$). For simplicity, we will drop the n label in the following.

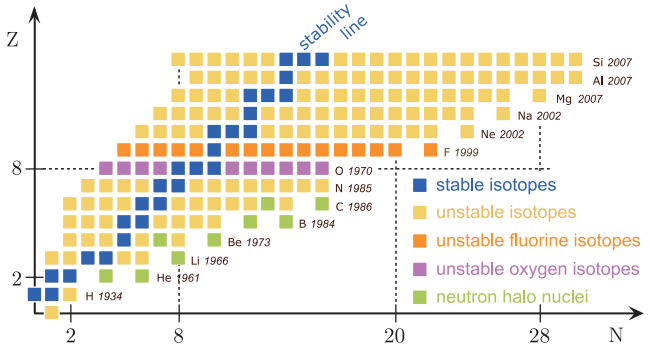

FIG. 1 (color online). Stable and unstable nuclei with $Z \leq 14$ and neutron number N [35]. The oxygen anomaly in the location of the neutron drip line is highlighted. Element names and years of discovery of the most neutron-rich nuclei are given. The axis numbers indicate the conventional magic numbers.

In Fig. 2, we show the single-particle energies (SPEs) of the neutron $d_{5/2}$, $s_{1/2}$ and $d_{3/2}$ orbitals at subshell closures $N = 8$, 14, 16, and 20. The evolution of the SPEs is due to interactions as neutrons are added. For the SPEs based on NN forces in Fig. 2(a), the $d_{3/2}$ orbital decreases rapidly as neutrons occupy the $d_{5/2}$ orbital, and remains well bound from $N = 14$ on. This leads to bound oxygen isotopes out to $N = 20$ and puts the neutron drip line incorrectly at ^{28}O. This result appears to depend only weakly on the renormalization method or the NN interaction used. We demonstrate this by showing SPEs calculated in the G matrix formalism [10], which sums particle-particle ladders, and based on low-momentum interactions $V_{\mathrm{low}\,k}$ [11] obtained from chiral NN interactions at next-to-next-to-next-to-leading order (N^{3}LO) [12] using the renormalization group. Both calculations include core polarization effects perturbatively [including diagram Fig. 3(d) with the Δ replaced by a nucleon and all other second-order diagrams] and start from empirical SPEs [13] in ^{17}O. The empirical SPEs contain effects from the core and its excitations, including effects due to 3N forces.

We next show in Fig. 2(b) the SPEs obtained from the phenomenological forces SDPF-M [13] and USD-B [14] that have been fit to reproduce experimental binding energies and spectra. This shows a striking difference compared to Fig. 2(a): As neutrons occupy the $d_{5/2}$ orbital, with N evolving from 8 to 14, the $d_{3/2}$ orbital remains almost at the same energy and is not well bound out to $N = 20$. The dominant differences between Figs. 2(a) and 2(b) can be traced to the two-body monopole components, which determine the average interaction between two orbitals. The monopole components of a general two-body interaction V are given by an angular average over all possible orientations of the two nucleons in orbitals lj and $l'j'$ [15],

$$V^{\mathrm{mono}}_{j,j'} = \sum_{m,m'} \langle jmj'm'|V|jmj'm'\rangle / \sum_{m,m'} 1, \qquad (1)$$

where the sum over magnetic quantum numbers m and m' can be restricted by antisymmetry (see [16,17] for details). The SPE of the orbital j is effectively shifted by $V^{\mathrm{mono}}_{j,j'}$ multiplied by the occupation number of the orbital j'. This leads to the change in the SPE and determines shell structure and the location of the drip line [16–19].

The comparison of Figs. 2(a) and 2(b) suggests that the monopole interaction between the $d_{3/2}$ and $d_{5/2}$ orbitals obtained from NN theories is too attractive, and that the oxygen anomaly can be solved by additional repulsive contributions to the two-neutron monopole components, which approximately cancel the average NN attraction on the $d_{3/2}$ orbital. With extensive studies based on NN forces, it is unlikely that such a distinct property would have been missed, and it has been argued that 3N forces may be important for the monopole components [20].

Next, we show that 3N forces among two valence neutrons and one nucleon in the ^{16}O core give rise to repulsive monopole interactions between the valence neutrons. While the contributions of the FM 3N force to other quantities can be different, the shell-model configurations composed of valence neutrons probe the long-range parts of 3N forces. The repulsive nature of this 3N mechanism can be understood based on the Pauli exclusion principle. Figure 3(a) depicts the leading contribution to NN forces due to the excitation of a Δ, induced by the exchange of pions with another nucleon. Because this is a second-order perturbation, its contribution to the energy and to the two-neutron monopole components has to be attractive. This is part of the attractive $d_{3/2} - d_{5/2}$ monopole component obtained from NN forces.

In nuclei, the process of Fig. 3(a) leads to a change of the SPE of the j, m orbital due to the excitation of a core nucleon to a Δ, as illustrated in Fig. 3(b) where the initial valence neutron is virtually excited to another j', m' orbital. As discussed, this lowers the energy of the j, m orbital and thus increases its binding. However, in nuclei this process is forbidden by the Pauli exclusion principle, if another neutron occupies the same orbital j', m', as shown in Fig. 3(c). The corresponding contribution must then be subtracted from the SPE change due to Fig. 3(b). This is taken into account by the inclusion of the exchange diagram, Fig. 3(d), where the neutrons in the intermediate

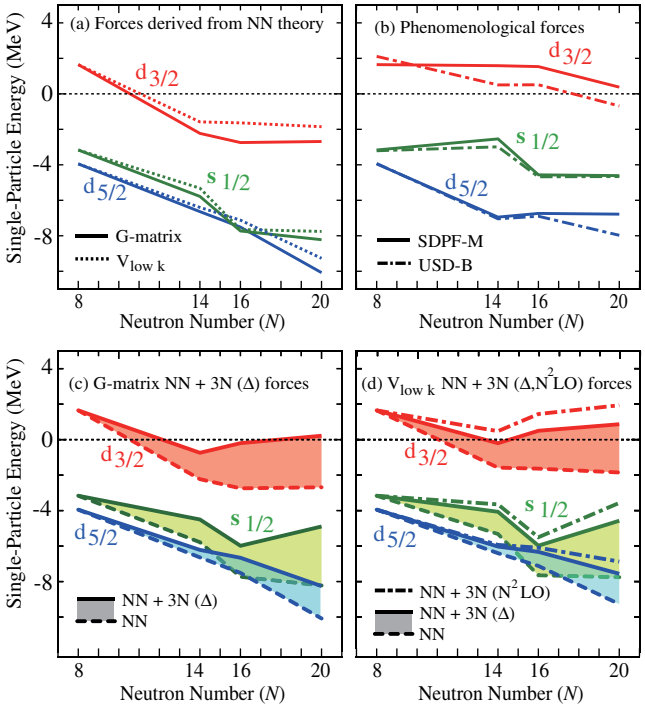

FIG. 2 (color online). Single-particle energies of the neutron $d_{5/2}$, $s_{1/2}$ and $d_{3/2}$ orbitals measured from the energy of ^{16}O as a function of neutron number N. (a) SPEs calculated from a G matrix and from low-momentum interactions $V_{\mathrm{low}\,k}$. (b) SPEs obtained from the phenomenological forces SDPF-M [13] and USD-B [14]. (c),(d) SPEs including contributions from 3N forces due to Δ excitations and chiral EFT 3N interactions at N^{2}LO [25]. The changes due to 3N forces based on Δ excitations are highlighted by the shaded areas.

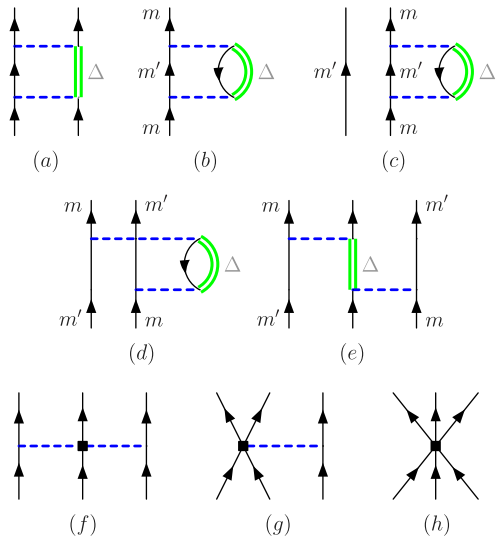

FIG. 3 (color online). Processes involving 3N contributions. The external lines are valence neutrons. The dashed and thick lines denote pions and Δ excitations, respectively. Nucleon-hole lines are indicated by downward arrows. The leading chiral 3N forces include the long-range two-pion-exchange parts, diagram (f), which take into account the excitation to a Δ and other resonances, plus shorter-range one-pion exchange, diagram (g), and 3N contact interactions, diagram (h).

state have been exchanged and this leads to the exchange of the final (or initial) orbital labels j, m and j', m'. Because this process reflects a cancellation of the lowering of the SPE, the contribution from Fig. 3(d) has to be repulsive for two neutrons. Finally, we can rewrite Fig. 3(d) as the FM 3N force of Fig. 3(e), where the middle nucleon is summed over core nucleons. The importance of the cancellation between Figs. 3(a) and 3(e) was recognized for nuclear matter in Ref. [21].

The process in Fig. 3(d) corresponds to a two-valence-neutron monopole interaction, schematically illustrated in Fig. 4(d). The resulting SPE evolution is shown in Fig. 2(c) for the G matrix formalism, where a standard pion-N-Δ coupling [22] was used and all 3N diagrams of the same order as Fig. 3(d) are included. We observe that the repulsive FM 3N contributions become significant with increasing N and the resulting SPE structure is similar to that of phenomenological forces, where the $d_{3/2}$ orbital remains high. Next, we calculate the SPEs from chiral low-momentum interactions $V_{\mathrm{low}\,k}$, including the changes due to the leading (N^{2}LO) 3N forces in chiral EFT [23], see Figs. 3(f)–3(h). We consider also the SPEs where 3N-force contributions are only due to Δ excitations [24]. The leading chiral 3N forces include the long-range two-pion-exchange part, Fig. 3(f), which takes into account the excitation to a Δ and other resonances, plus shorter-range 3N interactions, Figs. 3(g) and 3(h), that have been constrained in few-nucleon systems [25]. The resulting SPEs in Fig. 2(d) demonstrate that the long-range contributions due to Δ excitations dominate the changes in the SPE evolution and the effects of shorter-range 3N interactions are smaller. We point out that 3N forces play a key role for the magic number $N = 14$ between $d_{5/2}$ and $s_{1/2}$ [26], and that they enlarge the $N = 16$ gap between $s_{1/2}$ and $d_{3/2}$ [5].

The contributions from Figs. 3(f)–3(h) (plus all exchange terms) to the monopole components take into account the normal-ordered two-body parts of 3N forces, where one of the nucleons is summed over all nucleons in the core. This is also motivated by recent coupled-cluster calculations [27], where residual 3N forces between three valence states were found to be small. In addition, the effects of 3N forces among three valence neutrons should be generally weaker due to the Pauli principle.

Finally, we take into account many-body correlations by diagonalization in the valence space. The resulting ground-state energies of the oxygen isotopes are presented in Fig. 4. Figure 4(a) (based on phenomenological forces) implies that many-body correlations do not change our picture developed from the SPEs: The energy decreases to $N = 16$, but the $d_{3/2}$ neutrons added out to $N = 20$

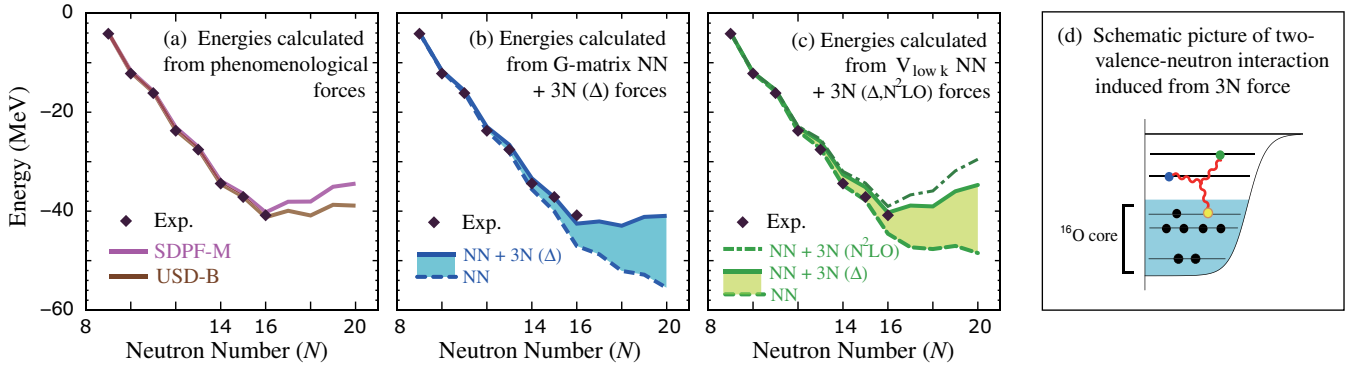

FIG. 4 (color online). Ground-state energies of oxygen isotopes measured from ^{16}O, including experimental values of the bound 16–24 O. Energies obtained from (a) phenomenological forces SDPF-M [13] and USD-B [14], (b) a G matrix and including FM 3N forces due to Δ excitations, and (c) from low-momentum interactions $V_{\mathrm{low}\,k}$ and including chiral EFT 3N interactions at N^{2}LO as well as only due to Δ excitations [25]. The changes due to 3N forces based on Δ excitations are highlighted by the shaded areas. (d) Schematic illustration of a two-valence-neutron interaction generated by 3N forces with a nucleon in the ^{16}O core.

remain unbound. Figures 4(b) and 4(c) give the energies derived from NN forces, using a G matrix or low-momentum interactions $V_{\mathrm{low}\,k}$, and including two-valence-neutron interactions due to $3N$ forces at the monopole level [28]. For all results based on NN forces, the energy decreases to $N = 20$ and the neutron drip line is incorrectly located at ^{28}O. The changes due to $3N$ forces based on Δ excitations are highlighted in Figs. 4(b) and 4(c). This leads to a better agreement with the experimental energies and to a kink at $N = 16$, which is further strengthened by shorter-range $3N$ forces, and for Fig. 4(c) leads to the neutron drip line at ^{24}O.

The same $3N$ forces lead to repulsion in neutron matter [29]. Our results are also consistent with early shell-model explorations with $3N$ forces up to ^{21}O, where a small repulsive effect as in Figs. 4(b) and 4(c) was found [30]. Because the formation of a halo is unrealistic for the $d_{3/2}$ orbital and $s_{1/2}$ is well bound [see Fig. 2(b)], it seems unlikely that the ground states beyond $N = 16$ become bound by including the coupling to the continuum. This is consistent with Ref. [31]. We plan to study $3N$-force effects on unbound states in the future using the methods of Refs. [31,32]. Fluorine isotopes have one more proton than oxygen, and NN forces, primarily the tensor part, with this proton provide more binding to the valence neutrons [19,33]. This valence proton-neutron effect is absent in the oxygen isotopes, making the repulsive $3N$ mechanism visible. Important directions for future work are to include the presented $3N$ contributions in coupled-cluster calculations [34] and in density-functional calculations, to systematically explore the effect over the full range of the nuclear chart.

In summary, we have presented a robust $3N$ mechanism that provides repulsive monopole interactions between valence neutrons. Using microscopic NN and $3N$ forces as well as known SPEs, our shell-model calculations naturally explain why ^{24}O is the heaviest oxygen isotope. The changes due to $3N$ forces are amplified and testable in neutron-rich nuclei and are expected to play a crucial role for matter at the extremes.

We thank S. Bogner, R. Furnstahl, A. Nogga, and T. Nakamura for useful discussions. This work was supported in part by grants-in-aid for Scientific Research (A) 20244022 and (C) 18540290, by the JSPS Core-to-Core program EFES, by EMMI and NSERC. TRIUMF receives funding via a contribution through the National Research Council Canada. Part of the numerical calculations have been performed at the JSC, Jülich, Germany.

[1] T. Baumann *et al.*, Nature (London) **449**, 1022 (2007).
[2] M. Langevin *et al.*, Phys. Lett. B **150**, 71 (1985); D. Guillemaud-Mueller *et al.*, Phys. Rev. C **41**, 937 (1990); M. Fauerbach *et al.*, Phys. Rev. C **53**, 647 (1996).
[3] H. Sakurai *et al.*, Phys. Lett. B **448**, 180 (1999).
[4] R. V. F. Janssens, Nature (London) **459**, 1069 (2009).
[5] A. Ozawa *et al.*, Phys. Rev. Lett. **84**, 5493 (2000); C. R. Hoffman *et al.*, Phys. Rev. Lett. **100**, 152502 (2008); R. Kanungo *et al.*, Phys. Rev. Lett. **102**, 152501 (2009).
[6] J. Fujita and H. Miyazawa, Prog. Theor. Phys.. **17**, 360 (1957).
[7] E. Epelbaum, H.-W. Hammer, and U.-G. Meißner, Rev. Mod. Phys. **81**, 1773 (2009).
[8] S. C. Pieper and R. B. Wiringa, Annu. Rev. Nucl. Part. Sci. **51**, 53 (2001); S. C. Pieper, Nucl. Phys. A **751**, 516 (2005).
[9] P. Navratil *et al.*, Phys. Rev. Lett. **99**, 042501 (2007).
[10] M. Hjorth-Jensen, T. T. S. Kuo, and E. Osnes, Phys. Rep. **261**, 125 (1995).
[11] S. K. Bogner, T. T. S. Kuo, and A. Schwenk, Phys. Rep. **386**, 1 (2003); S. K. Bogner *et al.*, Nucl. Phys. A **784**, 79 (2007).
[12] D. R. Entem and R. Machleidt, Phys. Rev. C **68**, 041001 (R) (2003).
[13] Y. Utsuno *et al.*, Phys. Rev. C **60**, 054315 (1999); Phys. Rev. C **70**, 044307 (2004).
[14] B. A. Brown and W. A. Richter, Phys. Rev. C **74**, 034315 (2006).
[15] R. K. Bansal and J. B. French, Phys. Lett. **11**, 145 (1964).
[16] E. Caurier *et al.*, Rev. Mod. Phys. **77**, 427 (2005).
[17] T. Otsuka *et al.*, Phys. Rev. Lett. **104**, 012501 (2010).
[18] T. Otsuka *et al.*, Phys. Rev. Lett. **87**, 082502 (2001).
[19] T. Otsuka *et al.*, Phys. Rev. Lett. **95**, 232502 (2005).
[20] A. P. Zuker, Phys. Rev. Lett. **90**, 042502 (2003).
[21] G. E. Brown and A. M. Green, Nucl. Phys. A **137**, 1 (1969).
[22] A. M. Green, Rep. Prog. Phys. **39**, 1109 (1976).
[23] U. van Kolck, Phys. Rev. C **49**, 2932 (1994); E. Epelbaum *et al.*, Phys. Rev. C **66**, 064001 (2002).
[24] The one-Δ contribution also corresponds to the leading (NLO) $3N$ force in an EFT with explicit Δ fields [7].
[25] S. K. Bogner *et al.*, arXiv:0903.3366.We use the $3N$ couplings fit to the ^{3}H binding energy and the ^{4}He radius for the smooth-cutoff $V_{\mathrm{low}\,k}$ with $\Lambda = \Lambda_{3N} = 2.0$ fm^{-1}. The one-Δ excitation $3N$ force corresponds to particular values for the two-pion-exchange part [7].
[26] M. Stanoiu *et al.*, Phys. Rev. C **69**, 034312 (2004).
[27] G. Hagen *et al.*, Phys. Rev. C **76**, 034302 (2007).
[28] The inclusion of multipole terms changes the oxygen ground-state energies by less than 300 keV.
[29] S. Fritsch, N. Kaiser, and W. Weise, Nucl. Phys. A **750**, 259 (2005); L. Tolos, B. Friman, and A. Schwenk, Nucl. Phys. A **806**, 105 (2008); K. Hebeler and A. Schwenk, arXiv:0911.0483 [Phys. Rev. C (to be published)].
[30] A. Polls *et al.*, Nucl. Phys. A **401**, 124 (1983); P. K. Rath *et al.*, Nucl. Phys. A **427**, 511 (1984).
[31] K. Tsukiyama, M. Hjorth-Jensen, and G. Hagen, Phys. Rev. C **80**, 051301(R) (2009).
[32] K. Tsukiyama, T. Otsuka, and R. Fujimoto, arXiv:1001.0729.
[33] Y. Utsuno *et al.*, Phys. Rev. C **64**, 011301(R) (2001).
[34] G. Hagen *et al.*, Phys. Rev. C **80**, 021306(R) (2009).
[35] G. Audi, A. H. Wapstra, and C. Thibault, Nucl. Phys. A **729**, 337 (2003).